JOURNAL OF MATERIALS SCIENCE 12 (1977) 1243–1252

Chemical vapour-deposited silicon nitride

Part 4 *Hardness characteristics*

KOICHI NIIHARA, TOSHIO HIRAI
The Research Institute for Iron, Steel and Other Metals, Tohoku University, Sendai, 980, Japan

The Vickers microhardness (VMH) of amorphous and crystalline chemical vapour-deposited silicon nitride (Pyrolytic-Si_3N_4) prepared under various deposition conditions using $SiCl_4$, NH_3 and H_2 has been measured at room temperature. The apparent VMH of Py–Si_3N_4 increases with decreasing indenter load, following the Meyer equation. For the amorphous Py–Si_3N_4, the VMH value at a load of 100 g ranges from 2200 to 3200 kg mm^{-2} depending upon deposition temperature (T_{dep}) and total gas pressure (P_{tot}). On the other hand, the VMH of the crystalline Py–Si_3N_4 does not depend upon T_{dep} and P_{tot} but is affected by the preferred orientation. The hardness of the deposition surfaces with the (1 1 0), (2 1 0) and (2 2 2) orientations is 3800 kg mm^{-2}, while that of the cross-section with the (0 0 1) orientation is 3100 kg mm^{-2}. The hardness of the crystalline Py–Si_3N_4 is also affected by the grain size. For the fine grained Py–Si_3N_4 (about 1 μm), the VMH varies from 4600 to 5000 kg mm^{-2}. The hardnesses of three types of Py–Si_3N_4 are discussed in comparison with those of other ceramics.

1. Introduction

In high-temperature engineering applications, silicon nitride (Si_3N_4) has superior properties such as low coefficient of expansion, high strength, good chemical stability and low coefficient of friction. These applications include dies for resistance sintering, ball bearings, components in high-temperature gas turbine engines and inert components in corrosive environments [1–4].

Products of Si_3N_4 are usually fabricated by reaction-sintering and hot-pressing techniques and thereby voids and some additives must be involved. Mechanical properties of the Si_3N_4 products depend strongly upon the purity, porosity and microstructure in a way similar to other ceramics [4–10].

One of the most important properties required for high-temperature structural materials is the high degree of surface hardness that results in good abrasion and erosion resistance. However, the hardness values of Si_3N_4 reported in the literature vary widely with the preparation techniques and conditions [4, 8–20]. The Vickers microhardness (VMH) at an applied load of 100 g is reported to be 1020 to 2200 kg mm^{-2} for the reaction-sintered Si_3N_4 [9, 13] and 1600 to 3800 kg mm^{-2} for the hot-pressed Si_3N_4 [4, 16].

Pyrolytic Si_3N_4 obtained by a chemical vapour deposition technique is expected to possess excellent properties as compared with the reaction-sintered and hot-pressed Si_3N_4. Nevertheless, there are very few systematic investigations on the mechanical properties of Py–Si_3N_4. In making an assessment of Py–Si_3N_4 for many potential applications, it is important to know its hardness characteristics. The only published value available for comparison is that of Kuntz *et al.* [19, 20] for Py–Si_3N_4, 2850 kg mm^{-2} at an undefined load.

As reported previously [21–23], the massive amorphous and crystalline Py–Si_3N_4 with thicknesses up to 4.6 mm have successfully been prepared in our laboratory, and the relations of the preparation conditions to the microstructure, density, deposition rate and crystal structure have been investigated. In the present work we report on the VMH values of Py–Si_3N_4 measured at

TABLE I Some properties of amorphous and crystalline Py–Si_3N_4

	Amorphous Py–Si_3N_4	Crystalline Py–Si_3N_4
Structure	Amorphous	α (hexagonal)
Colour	White (translucent)	White to black (translucent)
Density ($g\,cm^{-3}$)	2.60 to 2.89 (82 to 91% of D_{th}*)	3.15 to 3.18 (99 to 100% of D_{th}*)
Maximum deposition rate ($mm\,h^{-1}$)	0.36	0.73
Preferred orientation	–	(1 1 0), (2 1 0), (2 2 2)
Oxygen content (wt %)	2.2 to 1.6	1.1 to 0.3
Grain size (μm)		
(in C region)†	–	> 10
(in A–C boundary)†	–	~ 1

*D_{th}: a theoretical density of α-Si_3N_4, 3.18 $g\,cm^{-3}$.
† See Fig. 1.

room temperature and the effects of the microstructure, density and crystal orientation on the hardness.

2. Experimental procedure
2.1. Py–Si_3N_4 samples
The amorphous and crystalline Py–Si_3N_4 were deposited on a graphite substrate, using a mixture of NH_3, $SiCl_4$ and H_2. The preparation conditions were as follows: flow rates of NH_3, $SiCl_4$ (in liq.) and H_2 = 60, 0.8 and 700 $cm^3\,min^{-1}$, respectively, deposition temperature (T_{dep}) = 1100 to 1500° C and total gas pressure (P_{tot}) = 10 to 80 Torr. The procedure for the sample preparation has been reported in detail in a previous report [21]. Some properties of Py–Si_3N_4 used in the present experiment are summarized in Table I. Fig. 1 shows the relationship between the structure of Py–Si_3N_4 and the preparation conditions, T_{dep} and P_{tot} [21].

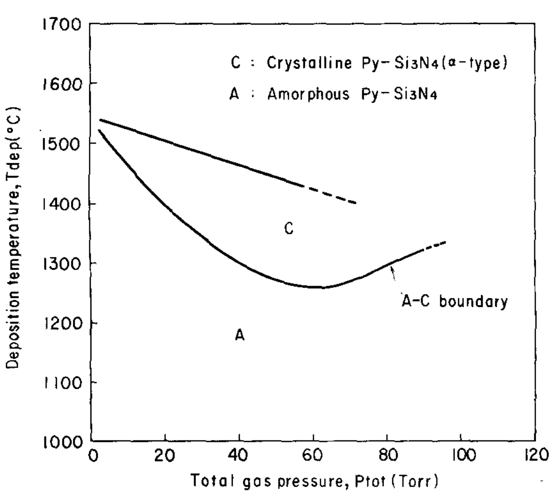

Figure 1 Effect of deposition temperature (T_{dep}) and total gas pressure (P_{tot}) on the structure of Py–Si_3N_4.

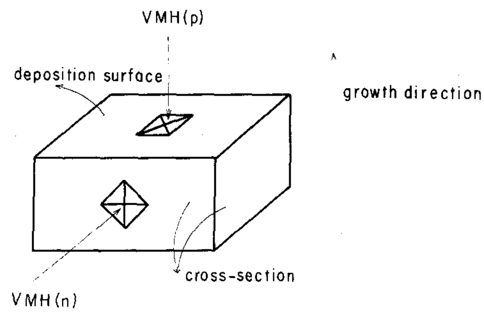

Figure 2 Two kinds of the indentations; $VMH_{(p)}$ and $VMH_{(n)}$ are the hardness values parallel and perpendicular to the growth direction, respectively.

2.2. VMH measurements
The Py-Si_3N_4 samples formed were mounted in resin, cut parallel and perpendicular to the deposition surface and polished with various grades of diamond paste to obtain a mirror-like surface for the measurements. As shown in Fig. 2, the VMH measurements of the deposition surface ($VMH_{(p)}$) and the cross-section ($VMH_{(n)}$) were made using an AKASHI diamond Vickers hardness tester (Model: MVK, Type: D, apex angle: 136°) equipped with an optical microscope (x 400). Further detailed observations of indentation diagonals were performed at a higher magnification of ~ x 3000 when necessary. Readings were successfully achieved by the use of polarized light and differential interference conditions. The indenter-loads of 25 to 300 g were applied for 30 sec and the relationship between the hardness and the load was determined. Almost all measurements were carried out using a load of 100 g. The VMH values reported in this work are the average of at least 20 indentations.

2.3. Relationship between VMH and the indenter load

In microhardness testing, VMH is given by the relationship:

$$\text{VMH} = 1854.4\, Pd^{-2} \ (\text{kg mm}^{-2}) \qquad (1)$$

where P is the load in g and d the length of the diagonal in μm. The relationship between P and d can be expressed empirically by the Meyer equation:

$$P = ad^{n} \qquad (2)$$

where a and n are constants depending upon the materials [24]. Thus, if the $\log P$ is plotted versus the $\log d$, the Meyer exponent n is obtained from the slope of a straight line. A relationship between VMH and P can be obtained from Equations 1 and 2 as follows:

$$\text{VMH} = 1854.4\, ad^{n-2} \ (\text{kg mm}^{-2}) \qquad (3)$$

Thus, VMH is independent of the load only when $n = 2$, while VMH increases and decreases with decreasing load when $n < 2$ and $n > 2$, respectively.

3. Results

3.1. Variation of VMH with indenter load

Fig. 3 shows the variation of VMH with the load for the amorphous Py–Si_3N_4 with the lowest hardness which was prepared at $T_{dep} = 1100°$ C and $P_{tot} = 40$ Torr. It is shown that the VMH values at loads of 300 and 25 g, VMH_{300} and VMH_{25}, are 2000 and 2400 kg mm^{-2}, respectively. On the other hand, as shown in Fig. 4, $VMH_{300} =$ 3200 kg mm^{-2} and $VMH_{25} = 6400$ kg mm^{-2} were obtained for the crystalline Py–Si_3N_4 with the highest hardness prepared at $T_{dep} = 1400°$ C and $P_{tot} = 20$ Torr. In both cases, VMH increases with decreasing load, according to the Meyer equation (Equation 2). Similar load dependence of VMH was observed in all the Py–Si_3N_4 samples. The load dependence is affected by the intrinsic hardness of each sample, as seen in Figs. 3 and 4. The values for the Meyer exponent n tend to decrease with increasing VMH, as summarized in Table II.

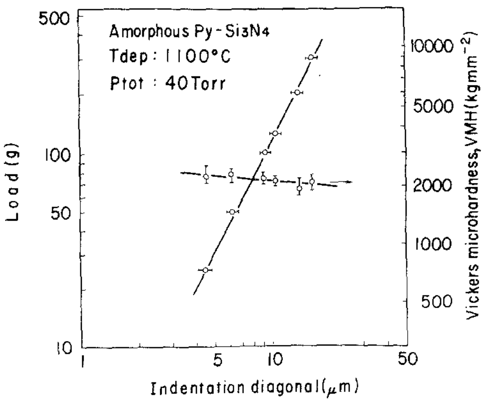

Figure 3 Relationship between Vickers microhardness and indenter load for amorphous Py–Si_3N_4 prepared at $T_{dep} = 1100°$ C and $P_{tot} = 40$ Torr.

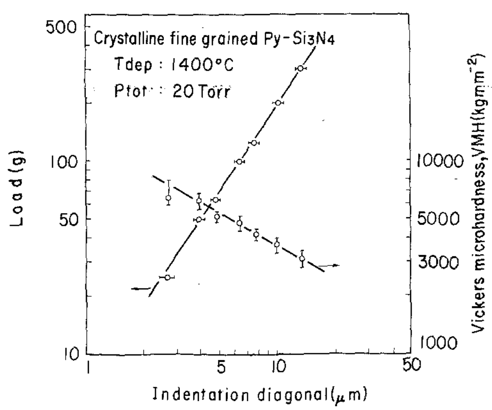

Figure 4 Relationship between Vickers microhardness and indenter load for fine grained crystalline Py–Si_3N_4 prepared at $T_{dep} = 1400°$ C and $P_{tot} = 20$ Torr.

TABLE II Values of the Meyer exponent of Py–Si_3N_4

Preparation conditions		Crystal structure*	Vickers microhardness, VMH_{100} (kg mm^{-2})	Meyer exponent, n
T_{dep} (° C)	P_{tot} (Torr)			
1100	40	A	2200	1.92
1200	10	A	3200	1.72
1200	40	A	2300	1.90
1300	10	A	3100	1.75
1400	20	A	2500	1.69
1300	60	C	3800 (p)†	1.68
1300	60	C	3100 (n)†	1.70
1400	20	C	4800	1.54

* A, amorphous; C, crystalline (α-Si_3N_4).
† p and n are the hardness parallel and perpendicular to the growth direction, respectively (see Fig. 2).

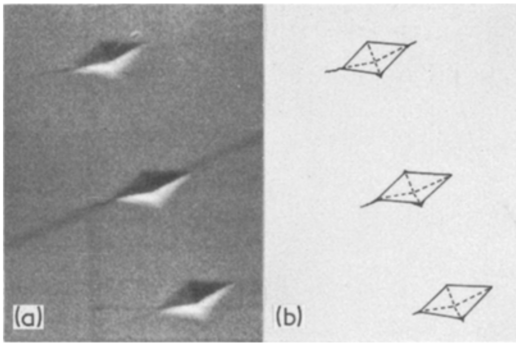

Figure 5 Scanning electron micrograph, taken in a direction at an angle of 60° from the direction of electron beam, of microhardness indentations at a 100 g load for the crystalline Py–Si_3N_4 prepared at $T_{dep} = 1300°$ C and $P_{tot} = 60$ Torr. (a) original, (b) sketched; diagonal ~ 7.0 μm.

Fig. 5 shows a scanning electron micrograph of indentations at 100 g load taken by inclining the surface to be observed at an angle of 60° to the direction of electron beam for the crystalline Py–Si_3N_4 prepared at 1300° C and 60 Torr. As outlined schematically in the sketch of Fig. 5b, the star-like cracks radiated from the corners of indentations. These cracks appear more predominantly at higher loads in the hard samples. Sometimes, edges of indentations were spalled out at high loads of 200 and 300 g.

3.2. The hardness of the deposition surface and the cross-section, $VMH_{(p)}$ and $VMH_{(n)}$

Hardness measurements were carried out on two kinds of surfaces, the deposition surface and the cross-section, as shown in Fig. 2. Fig. 6 shows the $VMH_{100,p}$ and $VMH_{100,n}$ values for the amorphous Py–Si_3N_4 prepared at $T_{dep} = 1300°$ C and $P_{tot} =$ 30 Torr and the crystalline Py–Si_3N_4 deposited at 1300° C and 60 Torr and at 1400° C and 40 Torr. The $VMH_{100,n}$ values are independent of the distance from the substrate-side surface, exept that the region in contact with the substrate (below 0.1 mm) in the crystalline Py–Si_3N_4 formed at 1400° C and 40 Torr, shows a decrease in hardness as indicated by △ in the figure. This means that the present samples are almost homogeneous. For the crystalline Py–Si_3N_4, $VMH_{100,p}$ is approximately 600 kg mm^{-2} higher than $VMH_{100,n}$ as marked ▲ and ■. However, there is a negligible difference in value between $VMH_{100,n}$ and $VMH_{100,p}$ for the amorphous Py–Si_3N_4.

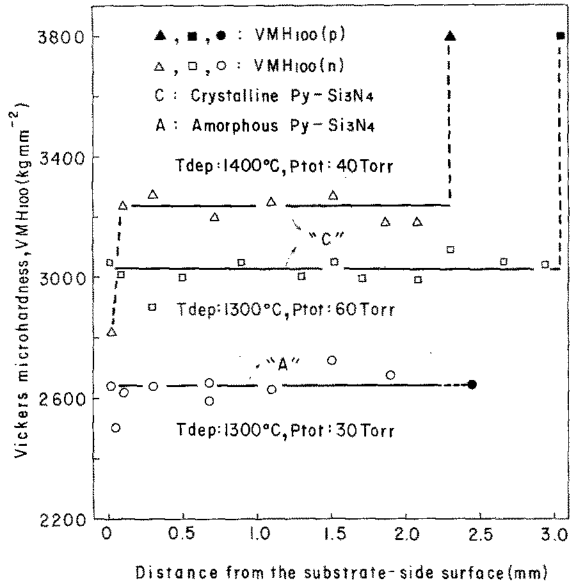

Figure 6 The Vickers microhardness on the deposition surface ($VMH_{100,p}$) and the cross-section ($VMH_{100,n}$) for Py–Si_3N_4 prepared at $T_{dep} = 1400°$ C and $P_{tot} =$ 40 Torr, $T_{dep} = 1300°$ C and $P_{tot} = 60$ Torr, and $T_{dep} =$ 1300° C and $P_{tot} = 30$ Torr. p and n, see Fig. 2.

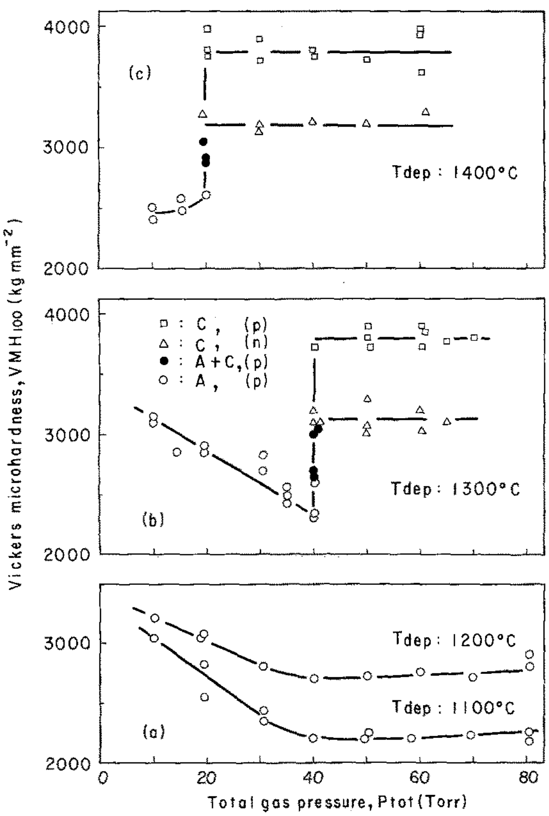

Figure 7 Effect of total gas pressure (P_{tot}) on Vickers microhardness (VMH_{100}). A, amorphous; C, crystalline (α-Si_3N_4); p and n, see Fig. 2.

3.3. Effect of total gas pressure on VMH

Fig. 7 represents the relationship between VMH_{100} and P_{tot} for the Py–Si_3N_4 samples prepared at T_{dep} of 1100 to 1400° C. In the case of the amorphous Py–Si_3N_4, only $VMH_{100,n}$ is plotted in Fig. 7 because of the almost identical values of $VMH_{100,p}$ and $VMH_{100,n}$. The $VMH_{100,p}$ of the amorphous Py–Si_3N_4 decreases with increasing P_{tot} in the range of 10 to 40 Torr as indicated by ○ in Fig. 7a and b. The maximum and minimum $VMH_{100,p}$ values of the amorphous Py–Si_3N_4 were 3050 and 2200 kg mm^{-2} at 1100° C, 3200 and 2700 kg mm^{-2} at 1200° C and 3100 and 2300 kg mm^{-2} at 1300° C, respectively. $VMH_{100,p}$ varies widely at 1300° C and 40 Torr (Fig. 7b) and at 1400° C and 20 Torr (Fig. 7c) corresponding to the A–C boundary condition (Fig. 1). This is the result of partial heterogeneous depositions of the amorphous and crystalline Py–Si_3N_4 by fluctuations in the preparation conditions during the deposition [21]. Although the data are not included in Fig. 7, the small grained portion (about 1 μm grain size) of the crystalline Py–Si_3N_4 produced in the A–C boundary region indicates high $VMH_{100,FG}$ values of 4600 to 5000 kg mm^{-2}, while the VMH_{100} values of the large grained portion (about 10 μm) are $VMH_{(p)}$ = 3800 kg mm^{-2} and $VMH_{(n)}$ = 3100 kg mm^{-2}.

The hardness of the crystalline Py–Si_3N_4 at 1300° C and above 40 Torr is independent of P_{tot}; $VMH_{100,p}$ = 3800 kg mm^{-2} and $VMH_{100,n}$ = 3100 kg mm^{-2} as shown in Fig. 7b. The variation of VMH_{100} with P_{tot} for the crystalline deposits at 1400° C and above 20 Torr is analogous to that at 1300° C, being $VMH_{100,p}$ = 3800 kg mm^{-2} and $VMH_{100,n}$ = 3200 kg mm^{-2}.

3.4. Effect of deposition temperature on VMH

The relation between VMH_{100} and T_{dep} is given in Fig. 8. For the amorphous Py–Si_3N_4, $VMH_{100,p}$ is particularly influenced by T_{dep}, as indicated by the curves a to e. The maximum $VMH_{100,p}$ appeared at T_{dep} 1200° C. In the case of the crystalline Py–Si_3N_4, different VMH_{100} versus T_{dep} relations exist for the samples designated by n, p and FG and are independent of P_{tot} as indicated by curves i, j and k; the values of $VMH_{100,n}$, $VMH_{100,p}$ and $VMH_{100,FG}$ are 3150, 3800 and 4800 kg mm^{-2}, respectively. Curves f, g and h were drawn from the results obtained at the A–C boundary.

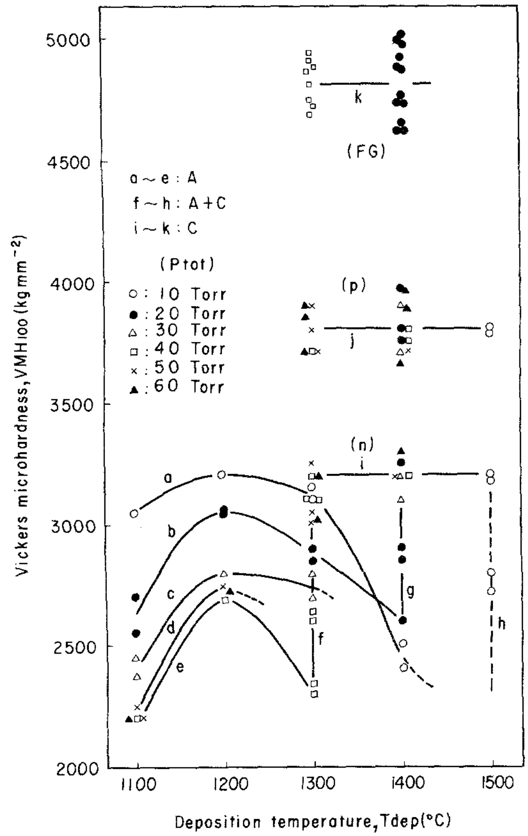

Figure 8 Effect of deposition temperature (T_{dep}) on Vickers microhardness (VMH_{100}). A, amorphous; C, crystalline (α-Si_3N_4); FG, fine grained; p and n, see Fig. 2.

3.5. Effect of density on VMH

Values of VMH_{100} are plotted as a function of density in Fig. 9. $VMH_{100,p}$ of the amorphous Py–Si_3N_4 deposited at T_{dep} of 1100 and 1200° C increases with density (▲, △), whereas $VMH_{100,p}$ at 1300 and 1400° C varies markedly in spite of the constant density (○, □) [22]. This shows that the density dependence of the hardness is affected by T_{dep}. For the crystalline Py–Si_3N_4, the density was very close to the theoretical value (3.18 g cm^{-3}) and was independent of the preparation conditions [22]. Three kinds of VMH_{100}, i.e. $VMH_{100,n}$, $VMH_{100,p}$ and $VMH_{100,FG}$, are independent of the density.

4. Discussion

4.1. Instrumental and reading errors in VMH measurements

Because of the indenter load dependence of VMH, the use of a standard load is essential when comparing hardness values. For the Py–Si_3N_4 sample with the highest hardness shown in Fig. 4,

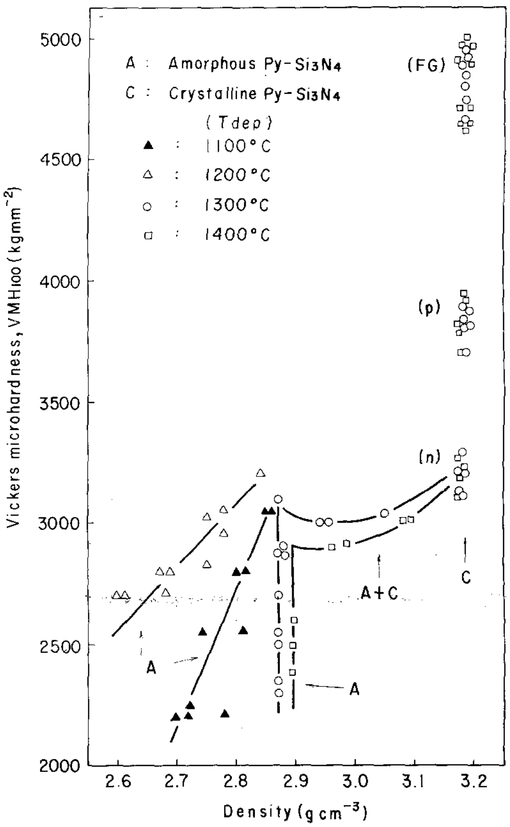

Figure 9 Effect of density on Vickers microhardness (VMH_{100}). FG, fine grained; p and n, see Fig. 2.

the loads below 50 g give rise to small diagonals, e.g. 4 μm at 50 g and 2.7 μm at 25 g. In the case of such small microhardness impressions, it is difficult to make detailed microscopic observations of the diagonals. As an alternative means, the diagonals were measured by enlarging the negatives of the micrographs (x 3000). At higher loads above 125 g, fractured (or spalled) indentations were obtained on the much harder samples. Almost all indentations on the crystalline Py–Si_3N_4 showed slightly fractured shapes, in which small cracks were generated at the corners of indentations as indicated in Fig. 5b. In consideration of the errors resulting from small indentations and crack formation, a load of 100 g was chosen as a standard load in the present VMH measurements. Moreover, since the present Py–Si_3N_4 samples are translucent, particular attention was directed to the conditions of optical microscopy, such as focusing and the intensity of radiation. The experimental error in measurements of the VMH values under the present experimental conditions was within ± 6%.

In order to attain accurate visual and instrumental observations, the hardness measurements of boron and $TiC_{0.88}$ were carried out under the same indentation conditions. These results are shown in Table III together with data from the literature [25–29]. The measured hardness values are in good agreement with the referenced ones.

4.2. The indenter load dependence of VMH

The hardness of ceramics generally depends upon the load in such a manner that it apparently increases with decreasing load. The relation between VMH and the load for various kinds of Si_3N_4 is shown in Fig. 10.

Pratt [9] reported $n = 1.48$ and 1.38 for the reaction-sintered α- and β-Si_3N_4, respectively. Noakes and Pratt [13] and Thompson and Pratt [10] reported that n of the reaction-sintered Si_3N_4 containing both the α- and β-phases was 1.4. Coe *et al.* [4] measured VMH of the hot-pressed Si_3N_4 with 1 wt% of MgO in the range of 100 to 1000 g and found that VMH decreased with increasing load. In this work the VMH values of Py–Si_3N_4 depended strongly upon the load, with the Meyer exponent n of the order of 1.54 to 1.92, and the load dependence of VMH became more pronounced in the samples with higher VMH as given in Table II. The values of n for Py–Si_3N_4

TABLE III The hardness of boron and titanium carbide

Material	Hardness ($kg\,mm^{-2}$)	V or K*	Load (g)	Reference
B	3400	V	50	25
B	2800	V	100	26
TiC	2988	V	30	25
TiC	2200, 2700	K	100	27
$TiC_{0.73-0.94}$	2060 to 2800	V	1000	28
$TiC_{0.96}$	2600	V, K	500	29
B	2760 ± 200	V	100	This work
$TiC_{0.88}$	2690 ± 160	V	100	This work

* V, Vickers microhardness; K, Knoop microhardness.

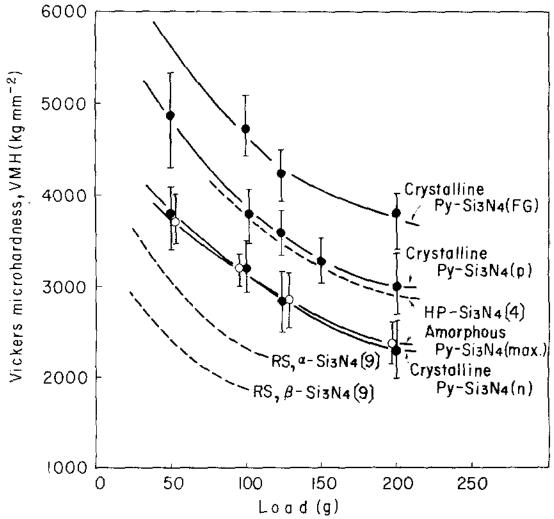

Figure 10 The load dependence of Vickers microhardness (VMH) for various kinds of Si_3N_4. RS, reaction-sintered; HP, hot-pressed; FG, fine grained; p and n, see Fig. 2.

are larger than those for the impure Si_3N_4 such as reaction-sintered and hot-pressed products.

The values of the Meyer exponent n for the transition metal oxides were reported by Wood and Hodgkiess [30] as follows: TiO_2 (1.72), Ta_2O_3 (1.85), Nb_2O_5 (1.48), Cu_2O (2.06), NiO (1.71), FeO (1.85 to 1.87), Fe_3O_4 (1.51 to 1.95), CoO (1.91), Cr_2O_3 (1.5 to 1.93) and ZnO (1.80 to 1.87). The load dependence of VMH is also observed in the case of hard refractory materials such as B_4C, ZrC, TiB_2, Al_2O_3, WC and SiC [9, 24]. In particular, the VMH values of WC and SiC varied markedly with load; the Meyer exponents n are 1.16 and 1.18 for WC and SiC, respectively [9].

4.3. VMH of amorphous Py–Si_3N_4

Bean *et al.* [31] measured the Knoop microhardness at a very low load of 8 g (KMH_8) and Mohs' hardness of the thin amorphous Py–Si_3N_4 films 1 μm thick prepared by pyrolysis of a SiH_4 + NH_3 + H_2 system. They reported that KMH_8 was dependent upon the NH_3 concentration of the gas mixture. At 0.6% NH_3, the amorphous Py–Si_3N_4 exhibited a maximum hardness, $KMH_8 = 3500$ kg mm^{-2}, which can possibly be converted to $VMH_{100} = 2400$ kg mm^{-2} by reference to the present load dependence of VMH and by using the empirical relations between VMH and KMH. They also reported that the Mohs' hardness increased with increasing T_{dep} up to 900° C, but independent of T_{dep} at 900 to 1200° C.

In the present work, the VMH_{100} value for the amorphous Py–Si_3N_4 was remarkably affected by the preparation conditions, especially T_{dep} and P_{tot}, and varied between 2200 and 3200 kg mm^{-2} (see Figs. 7 and 8). As shown in Fig. 9, the relationship between VMH_{100} and density differs depending upon T_{dep}. Yajima *et al.* [32] investigated the VMH values of pyrolytic graphite and siliconated pyrolytic graphite, and demonstrated that the VMH value is strongly influenced by the cross-links existing between the crystallites. In the present experiments, it appears that the VMH value of the amorphous Py–Si_3N_4 is affected by a structure which resembles that of cross-links. The nature of the growing cone of the amorphous Py–Si_3N_4 varied with P_{tot} [21], which seems to be related to the hardness (Fig. 7).

4.4. Effect of preferred orientations on VMH

As shown in Figs. 6 to 8, $VMH_{100,p}$ of the crystalline Py–Si_3N_4 was higher than $VMH_{100,n}$. As reported in Part 3 [23], it was observed that the crystalline Py–Si_3N_4 exhibited the marked (1 1 0), (2 1 0) and (2 2 2) orientations, and that the orientations varied from (1 1 0) and (2 1 0) to (2 2 2) with decreasing P_{tot} and with increasing deposition rate [23]. However, $VMH_{100,p}$ and $VMH_{100,n}$ were independent of T_{dep} and P_{tot}. From these facts, it is considered that the hardness of the (2 1 0) and (1 1 0) planes of α-Si_3N_4 are not different from that of the (2 2 2) plane, and that the difference between $VMH_{(p)}$ and $VMH_{(n)}$ is due to the presence of the (0 0 1) plane. Actually, the hardness of the (0 0 1) plane is lower than that of the (1 1 0) and (1 0 0) planes for α-Si_3N_4 single crystals prepared in our laboratory [33].

4.5 Effect of grain size on VMH

The relations between the hardness and the average grain size are represented by the Hall–Petch equation for grain-boundary hardening and the Cottrell equation for anti-phase boundary hardening [5–7, 34], respectively:

$$H = H_0 + K_H L^{-1/2} \qquad (4)$$

$$H = H_0 + K_C L^{-1} \qquad (5)$$

where H is the hardness, H_0, K_H and K_C are experimental constants and L is the grain size.

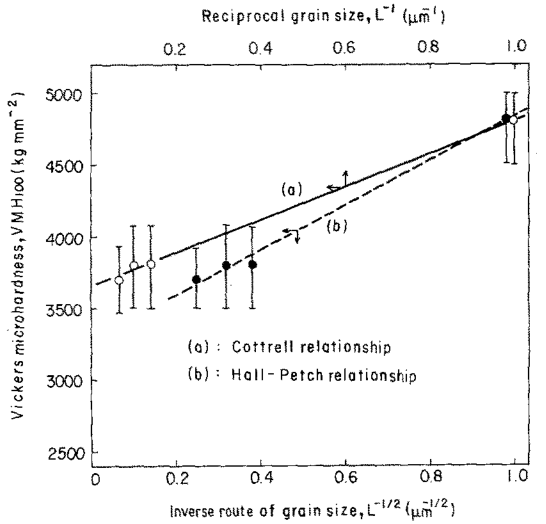

Figure 11 Effect of grain size on Vickers microhardness (VMH_{100}) for crystalline Py–Si_3N_4.

Fig. 11 shows the relationships between VMH_{100} (p and FG) of the crystalline Py–Si_3N_4 and the inverse square root ($L^{-1/2}$) and the inverse (L^{-1}) of grain size. In either case, the linear relationships are observed within experimental error. It is difficult to determine which model is better, because of the lower accuracy in the measurement of the grain size. For Equation 5, however, the extrapolation of the values to $L^{-1} = 0$ gives $H_0 = 3650$ kg mm^{-2} which is close to the hardness (VMH_{100} = 3600 kg mm^{-2}) of the (1 0 0) and (1 1 0) planes of α-Si_3N_4 single crystals [34].

Coe *et al.* [4] measured VMH of the theoretically dense and fine grained (0.3 to 0.6 μm) Si_3N_4 containing both α- and β-phases obtained by hot-pressing the α-Si_3N_4 powder with 1 wt% MgO. They reported that VMH_{100} was 3700 kg mm^{-2} and that the hardness increased with decreasing grain size. Although the grain size of the hot-pressed Si_3N_4 is smaller than that of Py–Si_3N_4 in the present work, VMH of the hot-pressed Si_3N_4 is lower than that of Py–Si_3N_4. This may be attributed to the vitreous phase ($MgSiO_3$) formed in the grain boundaries of the hot-pressed Si_3N_4 [35].

4.6. Comparisons of VMH between Py–Si_3N_4 and other refractory materials

The hardness values of Si_3N_4 prepared by various techniques are summarized in Table IV. The data listed are limited to the hardness measured at a load of 100 g, VMH_{100} and KMH_{100}, except for the hardness of Py–Si_3N_4. The hardness values reported in the literature are widely scattered, the cause of which seems to be fluctuations in purity, density, grain size, microstructure and crystal orientation of Si_3N_4 with the methods of production.

In Fig. 12, the VMH of the present Py–Si_3N_4 is compared with those of typical carbides, nitrides, borides and oxides [36–40]. As described above, the comparison of the hardness of different materials should be done at the same indenter load. Fig. 12 indicates that the present Py–Si_3N_4 samples are harder than the well-known hard materials such as TiC, W_2C, TiB_2 and Al_2O_3. Especially, the fine grained Py–Si_3N_4 is superior in hardness to B_4C.

TABLE IV Comparative hardness data on various kinds of Si_3N_4

Si_3N_4*	Phase and additive	Density† (g cm^{-3})	Orientation and grain size	VMH_{100} and KMH_{100}‡ (kg mm^{-2})	Reference
RS	α	2.1	–	2200	[9]
RS	β	2.1	–	1700	[9]
RS	$\alpha + \beta$ + Si	2.37 to 2.59	–	1020	[13]
HP	$\alpha + \beta$, 5 wt% MgO	3.12 to 3.18	–	1600 to 1800	[16]
HP	$\alpha + \beta$, 1 wt% MgO	3.17 to 3.19	0.3 to 0.6 μm	3700	[4]
HP	$\alpha + \beta$, 2.5 at% Ce_2O_3	3.18 to 3.22	2 to 3 μm	2550 to 2600 (KMH)	[18]
Py	α	3.07 to 3.18	(2 2 2), (0 0 2)	2850 (unknown load)	[19, 20]
Py	Amorphous	–	–	3500 (8 g load, KMH)	[31]
Py	Amorphous	2.60 to 2.90	–	2200 to 3200	This work
Py (p)§	α	3.18	(1 1 0), (2 1 0), (2 2 2) > 10 μm	3800	This work
Py (n)§	α	3.18	(0 0 2), > 10 μm	3100	This work
Py (FG)§	α	3.18	1 μm	4800	This work

* RS, reaction-sintered; HP, hot-pressed; Py, chemical vapour-deposited (Pyrolytic).
† The theoretical densities of α-Si_3N_4 and β-Si_3N_4 are 3.18 and 3.19 g cm^{-3}, respectively.
‡ VMH_{100}, the Vickers microhardness; KMH_{100}, the Knoop microhardness at 100 g load.
§ p and n, parallel and perpendicular to the growth direction, respectively; FG, fine grained.

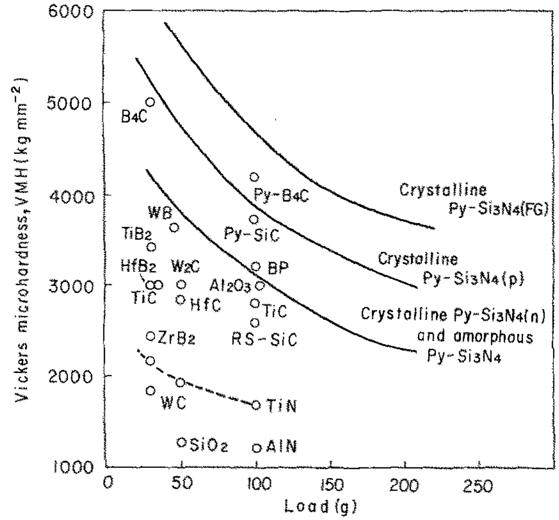

Figure 12 Comparative microhardness data on Py–Si_3N_4 and hard refractory materials. FG, fine grained; p and n, see Fig. 2.

5. Conclusions

(1) The Vickers microhardness (VMH) of Py–Si_3N_4 increased with decreasing indenter load. The Meyer exponent n varied from 1.54 to 1.92 depending upon the intrinsic hardness of each sample, and tended to be smaller in the harder Py–Si_3N_4.

(2) For the amorphous Py–Si_3N_4, the hardness was dependent upon the preparation conditions of the deposition temperature (T_{dep}) and the total gas pressure (P_{tot}). At T_{dep} of 1100 to 1300° C, the hardness decreased with increasing P_{tot} from 10 to 40 Torr. The maximum and minimum values of VMH_{100}, measured at a 100 g load, were 3200 kg mm^{-2} at 1200° C and 10 Torr, and 2200 kg mm^{-2} at 1100° C and 40 Torr, respectively. Moreover, the hardness of the amorphous Py–Si_3N_4 was related to the density.

(3) For the crystalline Py–Si_3N_4 (α-type), the hardness was independent of T_{dep} and P_{tot}, but it was affected by the preferred orientation. The $VMH_{100,p}$ value of the deposition surface with the (1 1 0), (2 1 0) and (2 2 2) orientations was 3800 kg mm^{-2}, while the $VMH_{100,n}$ value of the cross-section with the (0 0 1) orientation was 3100 kg mm^{-2}.

(4) The hardness of the crystalline Py–Si_3N_4 increased with decreasing grain size. For the fine grained (about 1 μm) Py–Si_3N_4 produced in the amorphous–crystalline boundary region, the $VMH_{100,FG}$ values ranged from 4600 to 5000 kg mm^{-2}.

Acknowledgement

This research was supported in part by the scientific research fund from the Ministry of Education, Contract Nos. 047015 and 075078.

References

1. N. L. PARR and E. R. W. MAY, *Proc. Brit. Ceram. Soc.* 7 (1967) 81.
2. D. J. GOODFREY, *Metals and Materials* **2** (1968) 305.
3. A. F. McLEAN, *Bull. Amer. Ceram. Soc.* **52** (1973) 464, 482.
4. R. F. COE, R. J. LUMBY and M. F. PAWSON, "Special Ceramics 5", edited by P. Popper (British Ceramic Research Association, Stoke-on-Trent, 1972) p. 361.
5. W. C. RILEY and J. H. RICHARDSON, "Modern Ceramics", edited by J. E. Hove and W. C. Riley (Wiley, New York, 1965) p. 177.
6. F. P. KNUDSEN, *J. Amer. Ceram. Soc.* **42** (1959) 376.
7. R. H. J. HANNINK and M. J. MURRAY, *Acta Met.* **20** (1972) 123.
8. J. A. COPPLA, R. C. BRADT, D. W. RICHERSON and R. A. ALLIEGRO, *Bull. Amer. Ceram. Soc.* **51** (1972) 847.
9. P. L. PRATT, "Mechanical Properties of Engineering Ceramics", edited by W. W. Kriegel and H. Palmour III (Interscience, New York, 1961) p. 507.
10. D. S. THOMPSON and P. L. PRATT, *Proc. Brit. Ceram. Soc.* 6 (1966) 37.
11. J. F. COLLINS and R. W. GERBY, *J. Metals* 7 (1955) 612.
12. V. F. FUNKE and G. V. SAMSONOV, *Z. Obshchil Khim.* **28** (1958) 267.
13. P. B. NOAKES and P. L. PRATT, "Special Ceramics 5", edited by P. Popper (British Ceramic Research Association, Stoke-on-Trent, 1972) p. 299.
14. T. F. FRANGOS, *Materials in Design Engineering* January (1958) 115.
15. P. POPPER and S. N. RUDDLESDEN, *Trans. Brit. Ceram. Soc.* **60** (1961) 603.
16. G. G. DEELEY, J. M. HERBERT and N. C. MOORE, *Powder Met.* 8 (1961) 145.
17. A. TSUGE, K. KOMEYA, H. HASHIMOTO, K. NISHIDA and T. ISHII, *Toshiba Rev.* **30** (1975) 1.
18. K. S. MAZDIYASNI and C. M. COOKE, *J. Amer. Ceram. Soc.* 57 (1974) 536.
19. F. GALASSO, U. KUNTZ and W. J. CROFT, *ibid* **55** (1972) 431.
20. U. E. KUNTZ, U.S. Pat. 3,226,194 (1965).
21. K. NIIHARA and T. HIRAI, *J. Mater. Sci.* **11** (1976) 593.
22. *Idem, ibid* **11** (1976) 604.
23. *Idem, ibid* **12** (1977) 1233.

24. N. C. DUNEGAN, "Mechanical Properties of Engineering Ceramics", edited by W. W. Kriegel and H. Palmour III (Interscience, New York, 1961) p. 521.
25. G. V. SAMSONOV, "High Temperature Materials, No. 2 Properties Index", edited by G. V. Samsonov (Plenum Press, New York, 1964) p. 181.
26. A. V. SEYBOLT, ASM, *Trans. Quart.* **52** (1966) 971.
27. R. D. KOESTER and D. MOAK, *J. Amer. Ceram. Soc.* **50** (1967) 290.
28. G. V. SAMSONOV, M. S. KOVALCHENKO, V. V. DZEMELINSKII and G. S. UPADYAYA, *Phys. Stat. Sol. (a)* **1** (1970) 327.
29. D. L. KOHLSTEDT, *J. Mater. Sci.* **8** (1973) 777.
30. G. G. WOOD and T. HODGKIESS, *Werkstoffe und Korrosion* **23** (1972) 766.
31. K. E. BEAN, P. S. GLEIN and R. L. YEAKLEY, *J. Electrochem. Soc.* **114** (1967) 733.
32. S. YAJIMA, T. HIRAI and T. HAYASE, *Tanso* No. 69 (1972) 41.
33. K. HIHARA and T. HIRAI, "Synopses of the 1976 Spring Meeting of the Japan Inst. Metals", p. 158.
34. N. J. PETCH, *J. Iron Steel Inst.* **174** (1953) 25.
35. S. WILD, P. GRIEVESON, K. H. JACK and M. L. LATIMER, "Special Ceramics 5", edited by P. Popper (British Ceramic Research Association, Stoke-on-Trent, 1972) p. 377.
36. C. W. FORREST, P. KENNEDY and J. V. SHENNAN, *ibid*, p. 99.
37. E. H. VOICE and V. C. SCOTT, *ibid*, p. 1.
38. J. E. HOVE, "Modern Ceramics", edited by J. E. Hove and W. C. Riley (Wiley, New York, 1965) p. 1, 327.
39. J. F. LYNCH, C. G. RUDERER and W. H. DUCKWORTH, "Engineering Properties of Selected Ceramic Materials" (The American Ceramic Society, Ohio, 1966).
40. S. MIERZEJEMSKS and T. NIEMYSKI, *J. Less-Common Metals* **8** (1965) 365.

Received 16 July and accepted 27 July 1976.